American Journal of Electrical Power and Energy Systems
2022; 11(1): 11-22
http://www.sciencepublishinggroup.com/j/epes
doi: 10.11648/j.epes.20221101.12
ISSN: 2326-912X (Print); ISSN: 2326-9200 (Online)

An Improved Dynamic Control and Resonance Damping for Voltage Source Inverters in Microgrids Through a Novel Active Damping Technique

Wei Zhang, Girmaw Teshager Bitew, Dehua Zheng, Solomon Netsanet Alemu*, Dan Wei, Xun Zhang

Microgrid R&D Centre, Goldwind Science & Technology Co., Ltd., Beijing, China

Email address:

sol14net@yahoo.com (S. N. Alemu), WeiZhang147258369@126.com (Wei Zhang)

*Corresponding author

To cite this article:

Wei Zhang, Girmaw Teshager Bitew, Dehua Zheng, Solomon Netsanet Alemu, Dan Wei, Xun Zhang. An Improved Dynamic Control and Resonance Damping for Voltage Source Inverters in Microgrids Through a Novel Active Damping Technique. *American Journal of Electrical Power and Energy Systems*. Vol. 11, No. 1, 2022, pp. 11-22. doi: 10.11648/j.epes.20221101.12

Received: March 10, 2022; **Accepted**: March 29, 2022; **Published**: April 8, 2022

Abstract: Microgrids have the potential to provide customers with improved power quality and reliability. However, there are technical challenges related to the operation and control of microgrids and the distributed energy source (DERs) that constitute them. Resonance caused by the low-pass filters connected to the voltage source inverters of the DERs is one of those issues in the operation of microgrids. This paper proposes a novel technique of Active Damping Algorithm (ADA) for resonance damping and improving the dynamic stability of a microgrid composed of multiple converter-interfaced DERs. The paper considers two cases; one is where the resistor and the filter capacitor are connected in parallel, and the other is where they are connected in series. The proposed active damping method is based on output current feedback with automatically calculated and adjusted damping coefficients to suppress resonance. The proposed method was verified through simulation and experimental tests carried out using PSCAD/EMTDS and an operational microgrid in Beijing, China. The results from both the experiment and simulation analysis showed that the devised method was able to achieve the intended target; where the filter resonance is effectively surpassed and the voltage and frequency dynamic responses are quite stable and within the acceptable range during large power changes in the microgrid system.

Keywords: Microgrid, Dynamic Control, Active Damping, DER, Filter, Resonance

1. Introduction

Voltage source converter (VSC) based electrical energy storage (ESS) systems have become popular elements of microgrids because of the advantages that VSC brings to the operation and controllability of microgrids [1]. A low-pass filter (LPF) is a key component of inverter-based distributed energy (DER) systems in microgrids. It tries to suppress the switching harmonics at the point of connection of the DER units to the microgrid network [2, 3]. The typical LPF is an inductor-capacitor (LC) filter. Coupling inductors and isolation transformers are also usually used. Thus, combining the coupled inductor and transformer inductance into one inductor, the filter can be regarded as an inductor-capacitor-inductor (LCL) filter. The LCL filter is designed to reduce the high-order harmonics on the grid side of VSC [1]. However, a poor filter design could cause increased distortion of the current waveform due to the resonance effect. The current harmonics can also cause transformer saturation. In addition, the resonance problem of the LCL filter may bring instability to the inverter-based system [4, 5]. Since the high-order LCL filter contains multiple resonance frequencies, the current harmonics generated by the active/passive load and the switching harmonics generated by the inverter will cause system resonance, which may lead to output current distortion, oscillation, and instability [5, 6]. At low resonance frequencies, the stability of the system will deteriorate [7]. Therefore, the inductor should be properly designed and the filter resonance should be damped. Nevertheless, designing a properly configured filter is a

challenging problem due to the number of technical factors that need to be considered related to resonance damping and system instability. Other factors such as cost, inductance and capacitance values, power loss, and filter performance degradation are also to be under consideration during the design [3].

A proper damping strategy is a critical component of the filter design. If the damping is improper, the interaction between multiple inverters of DER may cause harmonic instability. If the resonance frequency is close to the fundamental frequency, it will cause severe voltage distortion and harmonic current amplification.

The basic mechanism for suppressing resonance in parallel operation of converter-based DERs is passive damping (i.e., a damping resistor connected in series or parallel with the filter inductor and/or capacitor). Figures 8 and 12 are typical topologies for passive damping applications. Passive damping can suppress resonance under all conditions. The damping resistor should be able to avoid resonance problems in the lower and upper parts of the harmonic spectrum. Passive damping resistors can provide better damping due to their larger series resistance. However, when applying this passive damping method, problems of power level, damping requirements, and power loss are usually faced. Therefore, to solve these problems, it is preferable to use active damping methods.

Active damping can be provided with the concept of the virtual resistor connected in series or parallel to the filter capacitors and/or inductors. There are different active damping techniques implemented in VSC based DER system applications such as a derivative filtered capacitor and notch filter. The former active damping method is less sensitive to parameter variation, but it may not achieve higher stability margins on the given filter parameters. On the other hand, the latter one is sensitive to parameter variations as it needs prior information about grid impedance; but it is less expensive to implement [1]. To address those issues, active damping schemes based on the active disturbance rejection control method [8] and dual-current active damping control strategy [4, 9] are proposed, but complicated computing procedures are experienced for obtaining the parameters of the methods. Moreover, grid impedance variation has always been a major concern. To address such an issue, a control method based on the z-domain root contours and frequency-domain passivity theorem is presented in the study by Wang et al., 2015 [10]. However, determining the values of the damping coefficients is complex as it is difficult to accurately measure the grid impedance during different operational modes and generation levels of microgrids.

Thus, modifying the control algorithm without using a real resistor can achieve similar behaviour as in the passive damping application. However, the methods which have been used to determine the active damping parameters are based on complex methods to reach appropriate values.

This paper presents a novel active damping technique to suppress a wide spectrum of resonance by changing a single parameter in the derived function. The virtual resistor in the devised control method behaves in the same way as the actual resistor in passive damping so that it increases the appropriate values of the phase margin and gain margin of the system.

The paper begins by introducing a multiple DER microgrid with LCL filters. It continues by discussing the details of the methodology followed in the study including the presentation of the S-domain impedance-based analysis for the LPF circuit. Subsequently, two active damping methods are presented; one is an output current feedback method and the other is an output voltage feedback method. The respective methods are realized through a virtual resistor connected in series and parallel to the filter capacitor. The Constant functional value is chosen and adjusted in the first method to determine and improve the impedance characteristic of the control-converter-filter system. Results and their discussion are provided in the third chapter of the paper. Major conclusions from the findings are forwarded in the final part of the paper.

2. Methodology

2.1. Description of the System

Figure 1 presents the structure of a two DER microgrid system considered in this paper. The VSCs of the DERs are connected to the network through LPF. The second inductor (L_T) of the LPF is the combined inductance of the coupling inductor and the isolating transformer. Thus, the LPF is considered an LCL type filter.

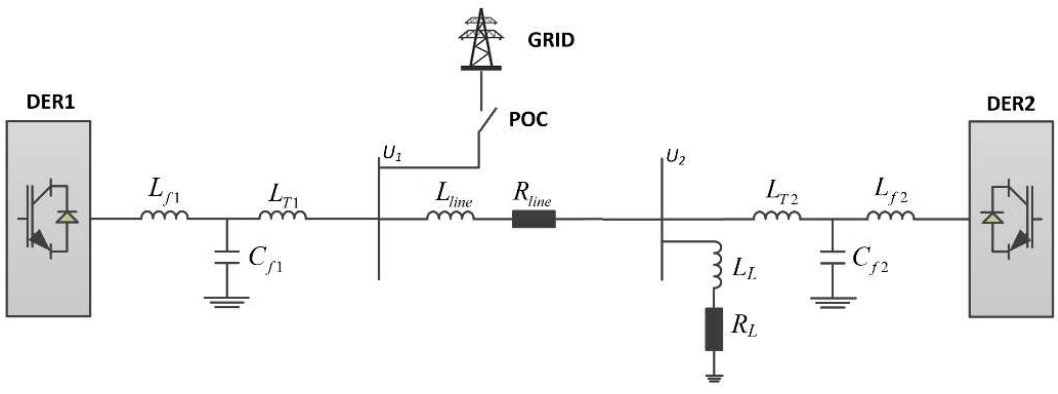

Figure 1. *LCL type LPF based VSC structure of a grid-connected microgrid with two DERs.*

As shown in Figure 1, DER1 is a lead-carbon battery with its converter, and DER2 is a supercapacitor (power-intensive energy storage) with its converter. L_{f1}, C_{f1}, and L_{T1} respectively represent the LPF inductance, capacitance, and the equivalent inductance of the isolating transformer for DER1. Similarly, L_{f2}, C_{f2}, and L_{T2} respectively represent the LPF inductance, capacitance, and the equivalent inductance of the isolating transformer for DER2. L_{line} and R_{line} represent the inductance and resistance of the lines respectively. However, in this paper, these parameters are neglected in the simulation model. POC is the point of connection between the microgrid and the utility grid. During the island operating mode of the microgrid, at least one of the DERs should be set in a grid forming source. During the grid-connected mode, the DERs can operate to control the power flow and can be set in a grid-following mode. The system voltage level of the microgrid bus is 400V. Using system parameters, mathematical modelling and tuning methods, the controller parameters are determined and listed in Table 1.

Table 1. *System parameters along with the PI control gains System parameters.*

System parameters					
Parameter	**value**	**Parameter**	**value**	**Parameter**	**value**
L_f	200µH	R_{line}	0Ω	u_{aO}	-10V
C_f	266µF	L_{line}	0H	f	50 Hz
L_t	65µH	k_{ii}	0.32	f_{sw}	3000 Hz
m	0.00622	k_{ip}	1.5^-4		
n	24^-6	k_{ui}	2.1		
L_L	0.2mH	k_{up}	105		
R_L	1.1Ω	u_{aD}	245V		

The purpose of the LCL filter is to reduce the high-order harmonics on the grid side, but due to the oscillation effect, poor filter design will cause more distortion. When the inductor is combined with the capacitor, it creates inherently a resonant frequency. The poles of high order resonant frequency can degrade the control performance. A poor bus voltage regulation could also happen in the case of a large coupling inductance. The resonant frequency affecting the total harmonic distortion (THD) can be defined in eq. (1).

$$f_{res} \approx \frac{1}{2\pi}\sqrt{\frac{L_f+L_t}{L_f L_t C_f}} \quad (1)$$

Substituting the parameters of the typical filter of Table 1 into (1), the frequency f_{res} is computed as 1.757kHz. This frequency is greater than 10 times the system frequency which complies with the thumb rule [3]. Nevertheless, it violates its relationship with the switching frequency. The switching frequency was chosen as 3000Hz for this paper including in both simulation and experimental cases as it is greater than half of it. If the resonance frequency is greater than half of the switching frequency, it will be the cause of instability. Based on eq. (1), it is possible to design the LPF having the resonant frequency not to be a severe cause of instability, but the experimental system we used for this paper is set with its paraments as shown in Table 1. Hence, it needs a control mechanism to address the problem.

2.2. Modelling of the Proposed Technique

2.2.1. LCL Type LPF

A typical LCL type LPF circuit diagram is shown in Figure 2. The equivalent transfer function of the current controller $G_i(s)$ is described as shown in the block diagram of Figure 3. With the absence of damping resistance R_d in the LPF, as shown in Figure 2, the transfer function of input voltage to the output current of the filter is given by eq. (2).

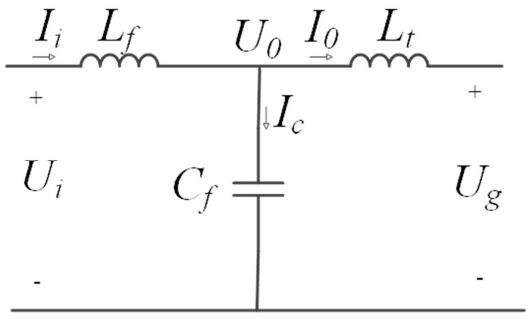

Figure 2. *Low-pass filter circuit.*

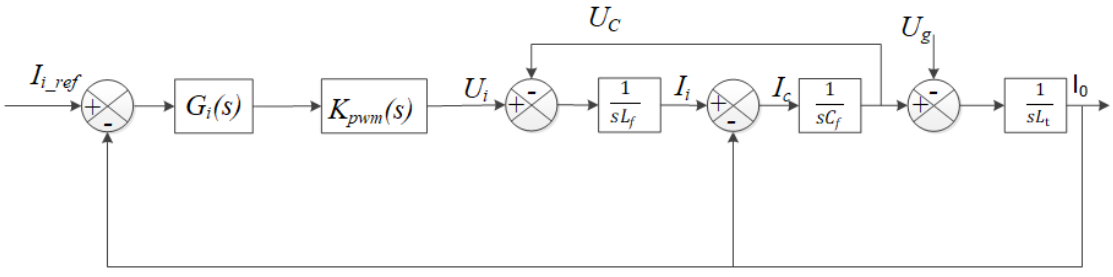

Figure 3. *Block diagram of transfer functions of the system with the current controller.*

The grid is assumed to be an ideal voltage source for the sake of computing the transfer function of the LCL LPF, and it represents a short circuit for harmonic frequencies. For the filter analysis, it is set to zero, i.e., $U_g = 0$. Thus,

$$H_1(s) = \frac{I_0}{U_i} = \frac{1}{s^3 L_f L_t C + s(L_f + L_t)} \quad (2)$$

The closed-loop form of the system is defined as

$$\frac{I_0}{I_{i\_ref}} = \frac{G_i(s)K_{pwm}(s)}{G_i(s)K_{pwm}(s)+s^3L_fL_tC+s(L_f+L_t)} \quad (3)$$

or

$$\frac{I_0}{I_{i\_ref}} = \frac{Z_{o1}(s)}{Z_{o1}(s)+Z_{o2}(s)} \quad (4)$$

where $Z_{o1}(s)=G_i(s)K_{pwm}(s)$ and $Z_{o2}(s)=s^3L_fL_tC+s(L_f+L_t)$; $K_{pwm}(s)$ represents the pulse width modulation as a time delay block.

Applying the principle of the current divider rule on eq. (4), the equivalent circuit is represented in Figure 4.

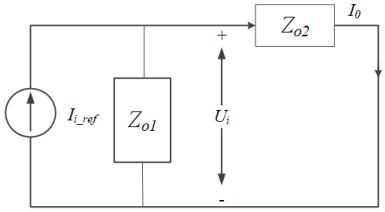

Figure 4. *Equivalent circuit diagram to represent Figure 3.*

The impedance characteristics of $Z_{o2}(s)$ of eq. (4) is shown in Figure 5. The current control system, shown in eq. (3), can be performed as demonstrated with the bode diagram as shown in Figure 6. The plot in Figure 6 shows an unstable system. This implies that when the DERs operate in parallel and are subjected to power sharing without a damping system, the microgrid becomes unstable. This is verified with the simulated results shown in Figure 7 as well. As it can be seen in figure 7, the two DERs started to share power at 0.8 sec, and voltage and frequency instability occurred after that due to the resonant frequency of the LPF which is disseminated in the network. This case is results illustrate the need for a damping system.

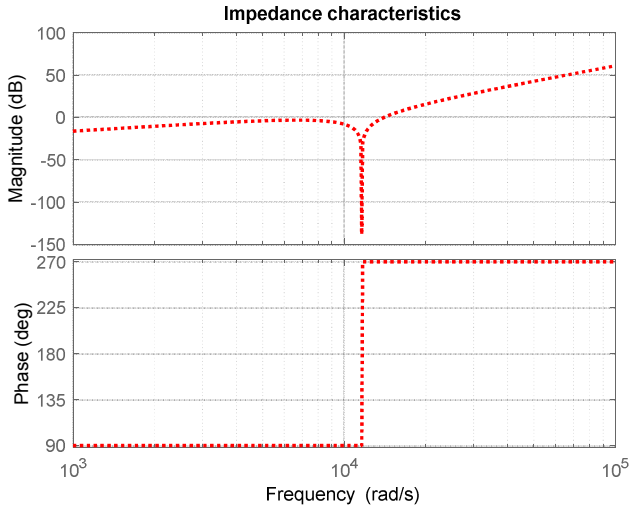

Figure 5. *Impedance characteristics of the filter system.*

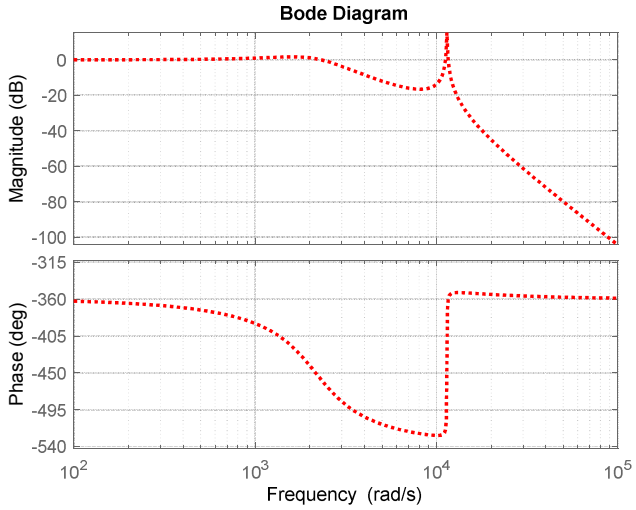

Figure 6. *Bode diagram of the current control system.*

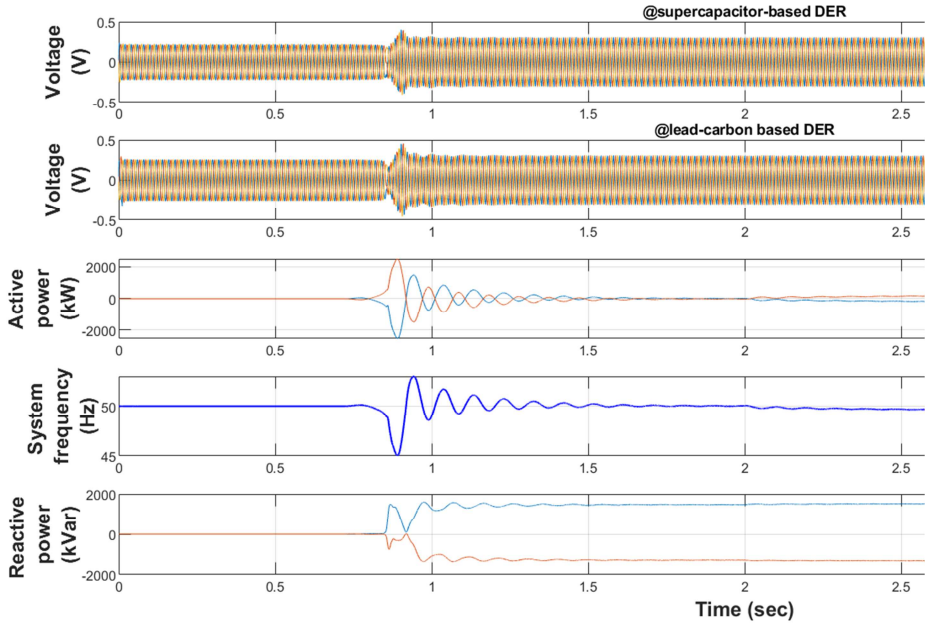

Figure 7. *The system response when operating without the damping method.*

2.2.2. Passive Damping for LCL Type LPF

The problem shown in Figure 7 can be addressed with the application of a passive damping system. Using passive damping connected in series or parallel to the LPF elements can have a significant effect. In this paper, two cases including series and parallel resistors connected with the filter capacitor are considered as depicted in Figures 8 and 12.

Implementing the damping resistor of Figure 8, the block diagram of the system transfer function including the control system will become as shown in Figure 9.

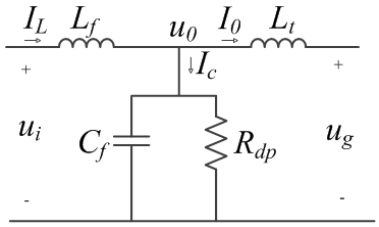

Figure 8. *Parallel resistor passive damping circuitry.*

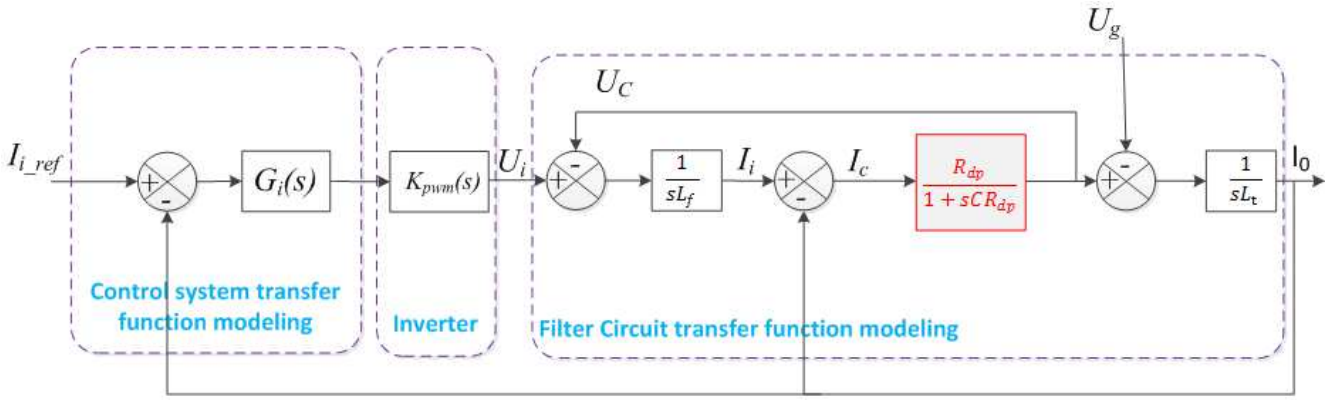

Figure 9. *Block diagram of transfer functions for the system with the current controller in the passive damping method.*

From Figure 9, the filter transfer function which describes the inverter output voltage versus its output current is defined as:

$$(s)=\frac{I_0}{U_i}=\frac{R_{dp}}{s^2L_fL_t(1+CR_{dp})+s((L_f+L_t)R_{dp}} \quad (5)$$

The value of R_{dp} can be estimated by using eq. (6) [1].

$$R_{dp}\approx\frac{1}{3*(2\pi f_{res})C_f} \quad (6)$$

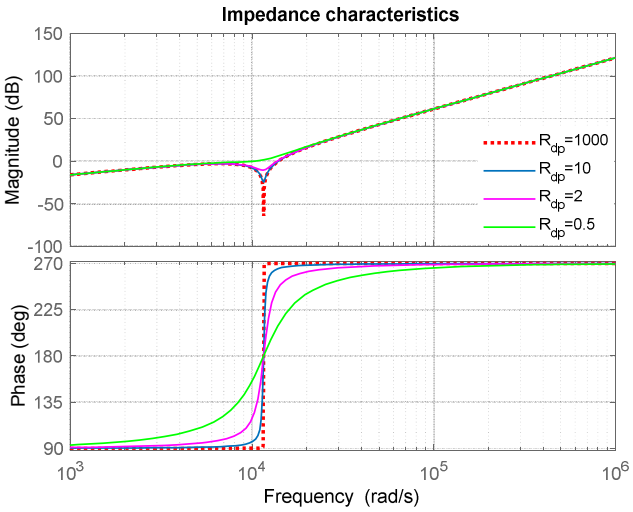

Figure 10. *The impedance characteristics of the filter for equation (5) with the different damping resistance values.*

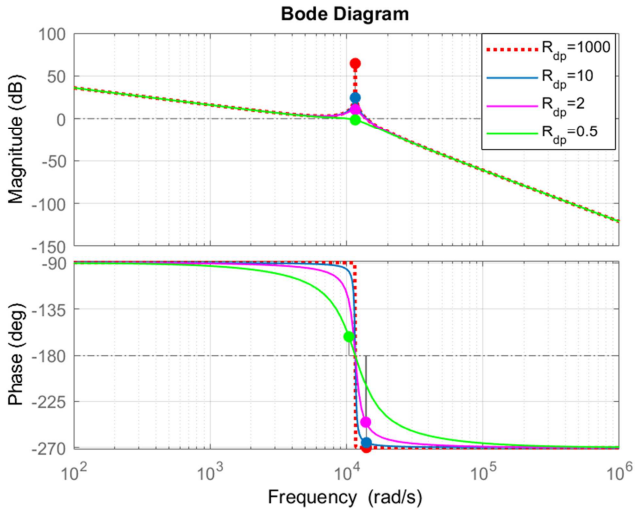

Figure 11. *The bode diagram of equation (5) with the different damping resistance values.*

Based on the transfer function of eq. (5), the impedance characteristics and the bode plot diagram are drawn as shown in Figures 10 and 11 respectively. The bode plot diagram depicts the effects of variation in damping resistance R_{dp}. Computed the damping resistance, the bode diagram has a negative gain margin and phase margin. Lowering the value of R_{dp}, we will get a larger phase and gain margins and will have a stable system. However, the impedance characteristic is not significantly affected by different resistance values except near the resonant frequency.

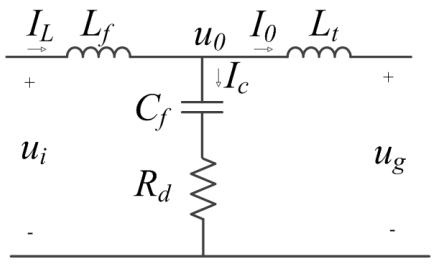

Figure 12. *Series resistor passive damping circuitry.*

From the topology of Figure 12, the transfer function of the filter describing the output current versus inverter output voltage is defined as:

$$H_2(s)=\frac{I_0}{U_i}=\frac{1+CR_ds}{s^3L_fL_tC+s^2(L_f+L_t)CR_d+s((L_f+L_t)} \quad (7)$$

Figure 13 illustrates the bode plot diagrams of the transfer function in eq. (7) to show the effects of damping resistance. The results show that such an arrangement of damping resistance provides a wide range of stable region, though the larger the damping resistance is the larger phase and gain margins.

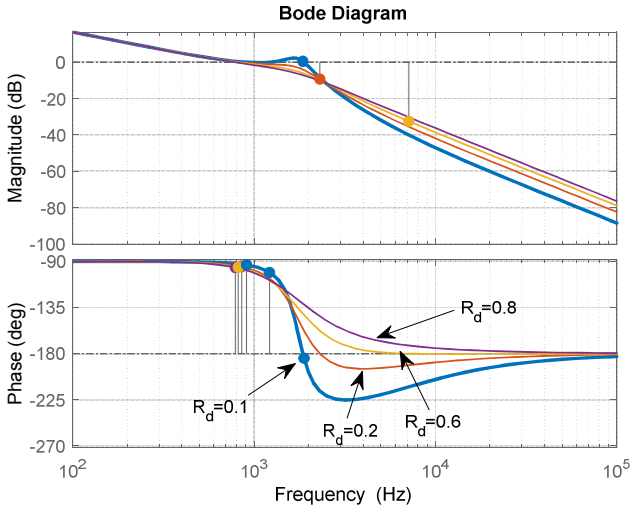

Figure 13. *The bode diagram of equation (7) with the different damping resistance values.*

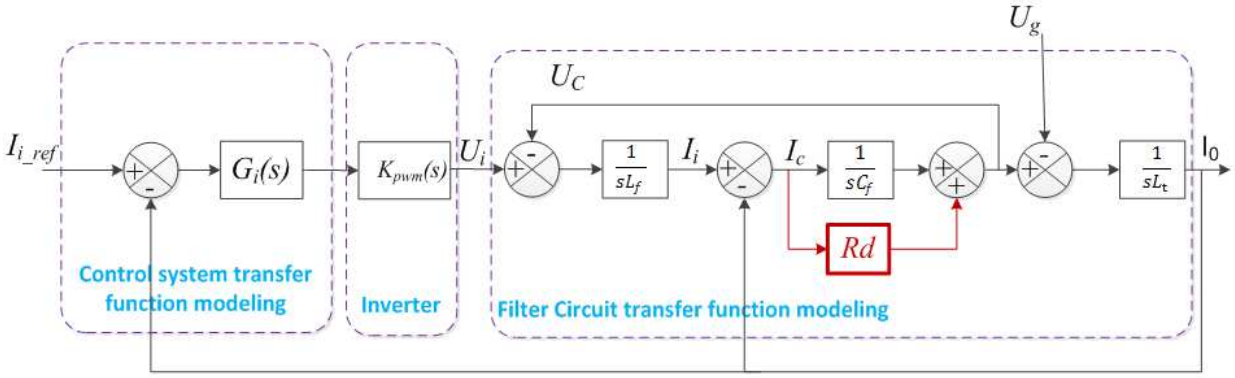

Figure 14. *Block diagram of transfer functions of the system with the current controller in a series resistor of passive damping method.*

2.2.3. Active Damping for LCL Type LPF

There are different active damping methods such as notch filter, and derivative filtered capacitor current methods that are used to address the issues related to passive damping methods. The former type is less expensive to implement, but it is sensitive to parameter variations and requires prior information about grid impedance. The latter one is less sensitive to parameter variation, but it may not achieve higher stability margins based on filter parameters.

Another active damping method is using the LPF output current as a feedback term to the current control loop. Figure 15 describes this method. The function G_{ad1} *(s)* is determined by testing its effect on the impedance characteristic and stability of the system. In this paper, the constant function is chosen for having a reasonable damping effect along with improving the impedance characteristic of the system.

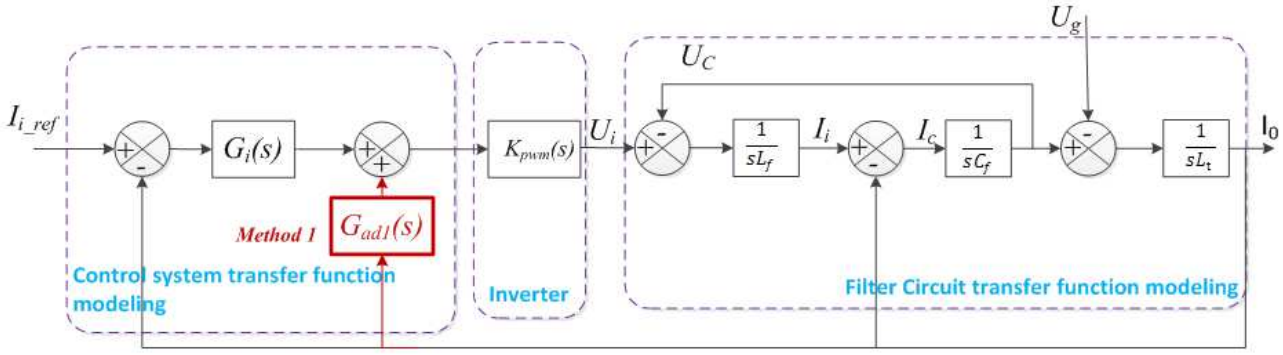

Figure 15. *The block diagram of the current control loop with the output current feedback damping method.*

The effect of the damping loop corresponds to the characteristics of the LCL-filter impedance, which can be readily derived using block diagram algebra [12], and the corresponding equivalent circuits of the active-damped LCL filter can be obtained. The impact of this damping method on the control system stability can be analysed. The equivalent filter circuit diagram, as shown in Figure 16, can be determined by considering the inner loop (current control) of Figure 15.

The transfer function is computed as:

$$\frac{I_0}{I_{i\text{-}ref}}=\frac{G_i(s)K_{pwm}(s)}{G_i(s)K_{pwm}(s)+s^3CL_fL_t+s(L_f+L_t)-G_{ad1}K_{pwm}(s} \quad (8)$$

or

$$\frac{I_0}{I_{i\text{-}ref}}=\frac{Z_{o1}(s)}{Z_{o1}(s)+Z_{o2}(s)} \quad (9)$$

where $Z_{o1}(s)=G_i(s)K_{pwm}(s)$ and $Z_{o2}(s)=s^3CL_fL_t+s(L_f+L_t)-G_{ad1}K_{pwm}(s)$

Thus, the equivalent filter circuit diagram is illustrated in Figure 16.

Accordingly, the transfer function for the output current vs inverter output voltage is derived and expressed as

$$H_4(s)=\frac{I_0}{U_i}=\frac{1}{s^3CL_fL_t+s(L_f+L_t)-G_{ad1}(s)K_{pwm}(s)} \quad (10)$$

Such damping circuity can effectively enhance the lowering of gain margin while power flowing varies in the system. $G_{ad1}(s)$ is defined by a constant term and its main role is to damp the oscillation as a resistor does. The value can be determined based on the level of damping. As shown in Figure 17, the impedance characteristic is changed when the damping value is varied. As the damping value increases, the stability decreases since the impedance phase poorly affects the power flow.

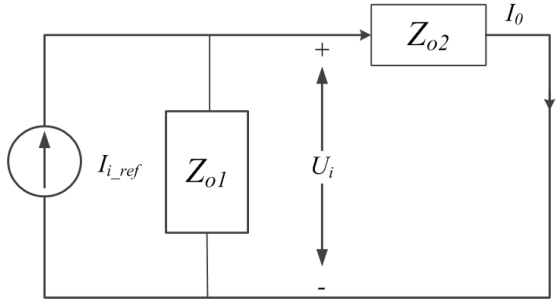

Figure 16. *The circuit diagram representation for active damping.*

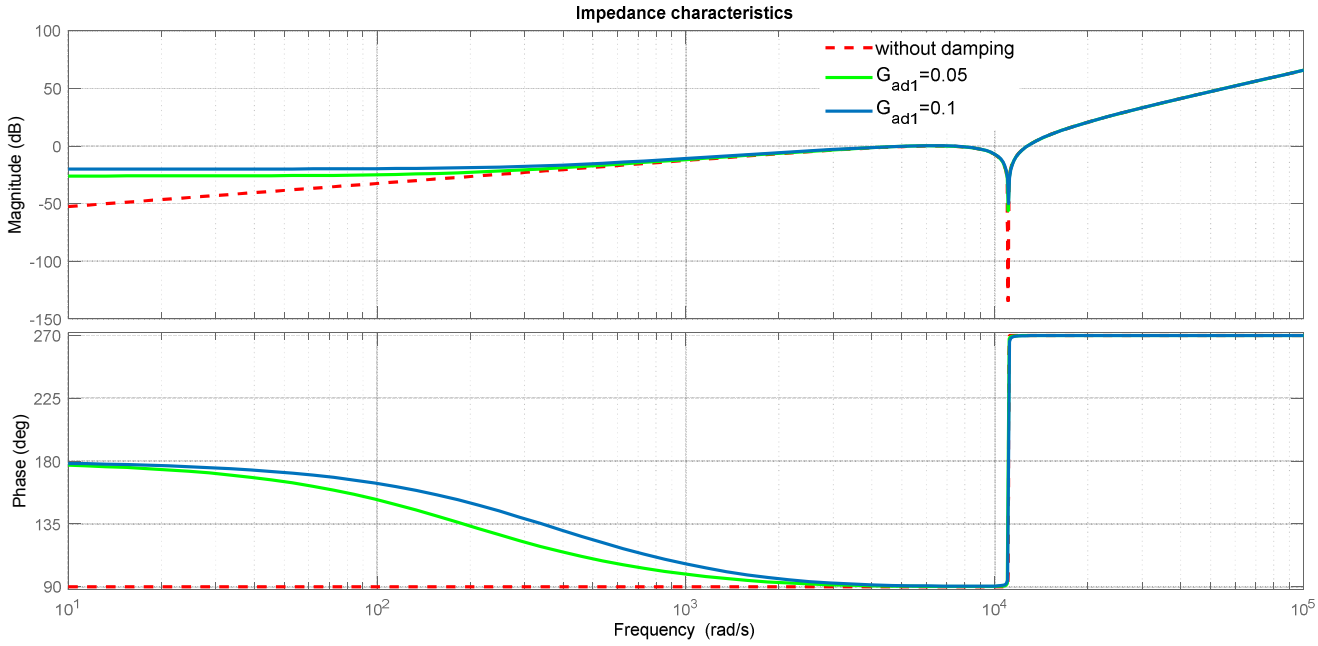

Figure 17. *The characteristics of system filter admittance for equation (7.49) with and without active damping.*

The simulation and experimental tests are carried out for this method and the results are illustrated in Figures 18a and 18b respectively.

As presented in Figure 17, the active damping method 1 performed well to suppress dynamic disturbance in the microgrid. However, the filter output current feedback based active damping method cannot handle disturbances when the power flow in the microgrid network becomes larger as shown in Figure 18. Even though the amplitude margin is well regulated by this damping method, the phase margin is decreased as the resonant frequencies exist while the power flow becomes larger. The simulated and experimental results show that as power flow increases, the resonance will be significant and the system becomes unstable. The dynamic disturbance boundary in the simulation and the experimental tests performed in this paper was 300 kW.

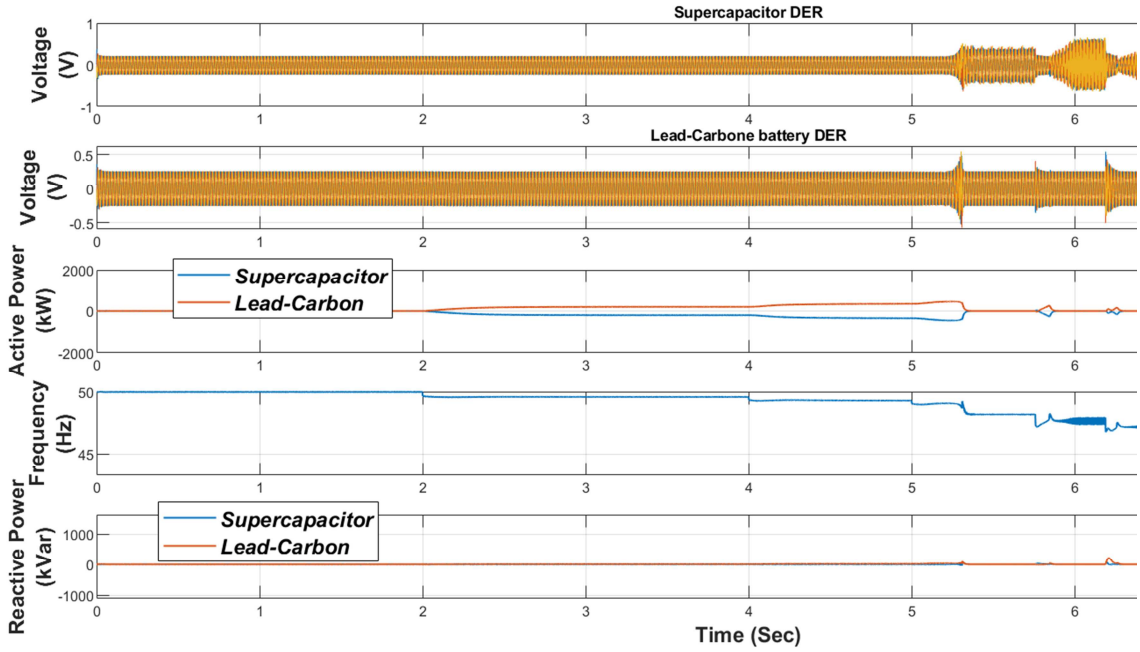

(a)

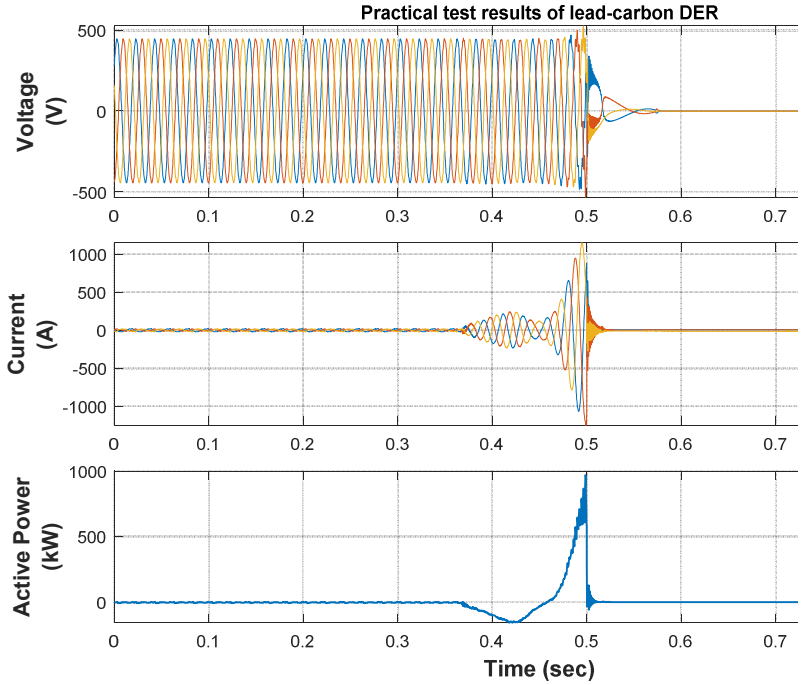

(b)

Figure 18. *Voltage, power, and frequency responses of the system when the active damping method of Figure 15 is applied;(a) simulation responses, (b) experimental responses.*

Thus, the output-voltage-feedback method is applied to eliminate the oscillating frequencies which cause the instability (as shown in Figure 18) to increase mainly the phase margin and gain margin as well. This method has a high-pass feature, which is capable to suppress the high resonant frequencies. It brings a big impact on the operation specially when there is high power flow in the network. To achieve this objective, a virtual resistor connected in series with the filter capacitor is taken into consideration to derive the active damping algorithm (ADA) method. Resonance problems in the lower and upper parts of the harmonic spectrum can be avoided by this damping method as the passive damping method does.

The derivation of this method is made based on the passive damping system illustrated in Figure 14. According to this figure, an approximate circuit diagram is drawn to represent the equivalent passive damping circuit.

Based on Figure 14, the transfer function of the system is

expressed by

$$\left[\left(I_{i_{ref}}\text{-}I_0\right)G_i(s)\right]K_{pwm}(s)=U_C+sL_fI_i \quad (11)$$

$$\text{But, } U_C=sL_tI_0 \text{ and } I_i=I_c+I_0 \quad (12)$$

Thus,

$$\left[\left(I_{i_{ref}}\text{-}I_0\right)G_i(s)\right]K_{pwm}(s)=sL_tI_0+sL_f(I_c+I_0) \quad (13)$$

Based on Figure 14, I_c has a relationship with U_c as $U_c = I_c/sC + R_dI_c$

$$I_c=\frac{sCU_c}{1+sCR_d} \quad (14)$$

Substituting (14) into (13), computing with (12) and rearranging the terms, we can obtain

$$\left[\left(I_{i_{ref}}\text{-}I_0\right)G_i(s)\right]K_{pwm}(s)+ K_{ad2}(s)U_c= sL_tI_0+ sL_fI_0+s^3CL_fL_tI_0 \quad (15)$$

where $K_{ad2}(s)=\left(\frac{s^3CL_f}{s+(1/CR_d)}\right)=k_hs^2\left(\frac{s}{s+\omega_h}\right)$; and $\omega_h=1/CR_d$ and $k_h=CL_f$

$K_{ad2}(s)$ is featured with a high-pass element, but it also needs to reflect the influence of the filter capacitor and inductance in the closed system. That is why it contains the term s^2.

$K_{pwm}(s)$ represents the converter of delay time. Thus, we need to put the damping element $K_{ad2}(s)$ before the block $K_{pwm}(s)$ as shown in Figure 19. Hence, $G_{ad2}(s)$ is defined as

$$G_{ad2}(s)=K_{ad2}(s)/K_{pwm}(s) =k_i\frac{s^3(s+\omega_1)}{s+\omega_2} \quad (16)$$

where, $k_i=1.5TCL_f$, $\omega_1=1/1.5T$ and $\omega_2=1/CR_d$, T is switching period.

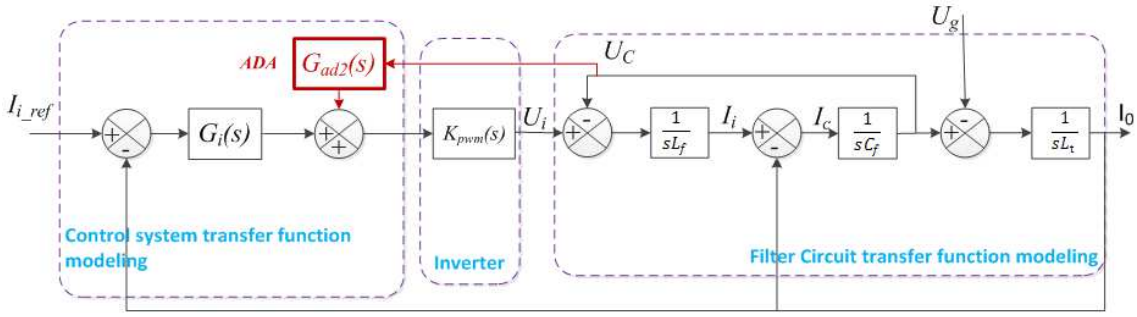

Figure 19. *The block diagram of the current control loop with the output voltage feedback damping method.*

Thus, the effect of the damping loop is equivalent to the shaping of LCL-filter admittance [13], which is algebraically derived above, and the corresponding equivalent circuit of active-damped LCL filter is obtained. The impact of the damping loop on the control system sensitivity function is already analysed in the section on the passive damping method.

To make the microgrid system operate in the wide range of frequency spectrum, power flow along with having regulated impedance characteristics, the two active damping methods are taken together as shown in Figure 20.

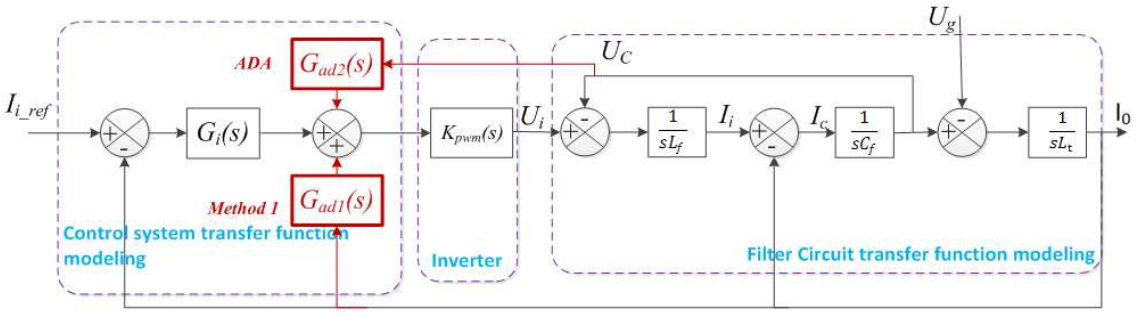

Figure 20. *The block diagram of the current control loop with the two damping methods.*

Thus, the transfer function of the current loop of Figure 20 for the output current versus inverter output voltage is computed as in eq. (17).

$$\frac{I_0}{I_{i\text{-}ref}}=\frac{G_i(s)K_{pwm}(s)}{G_i(s)K_{pwm}(s)+s^3CL_fL_t+s(L_f+L_t)-G_{ad1}(s)K_{pwm}(s)-sL_tK_{ad2}(s)} \quad (17)$$

From eq. (17), the equivalent filter circuit diagram is derived as shown in Figure 21.

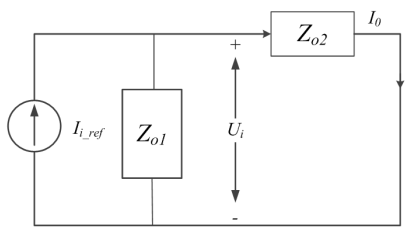

Figure 21. *Circuit diagram for active damping method of eq. (17).*

Hence, the transfer function for the output current versus inverter output voltage of the current loop of Figure 21 is computed as in eq. (18).

$$\frac{I_0}{I_{i\text{-}ref}} = \frac{Z_{o1}(s)}{Z_{o1}(s)+Z_{o2}(s)} \tag{18}$$

where $Z_{o1}(s)=G_i(s)K_{pwm}(s)$ and $Z_{o2}(s)=s^3CL_fL_t+s(L_f+L_t)-G_{ad1}(s)K_{pwm}(s)-sL_tK_{ad2}(s)$

Such a damping method can effectively enhance the gain and phase margins. As the results presented in Figures 22 and 23 illustrate, the combination of the two methods resulted in improved characteristics of output impedance and applicability to a wide range of frequencies including at resonance frequency.

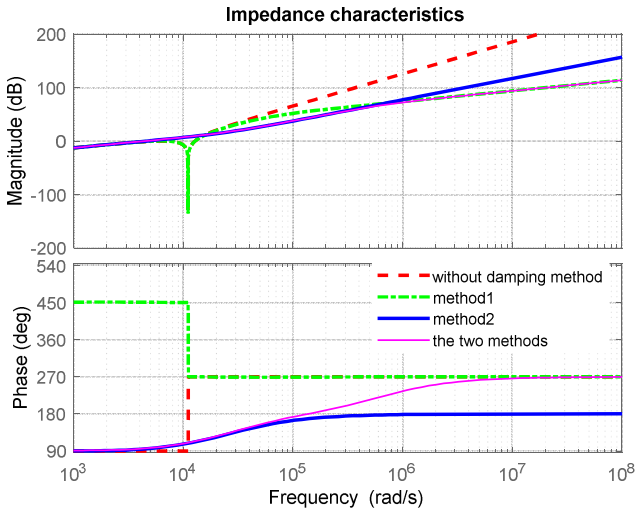

Figure 22. *Output impedance characteristics of the system.*

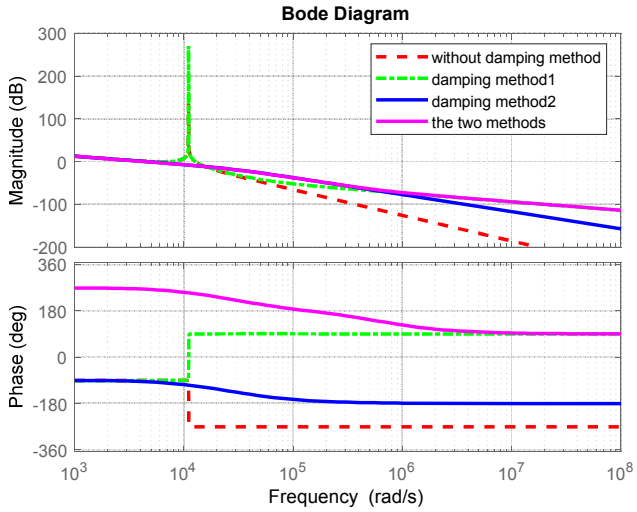

Figure 23. *The bode diagram of the system with different methods.*

3. Results and Discussion

3.1. Results

This section provides the simulation and experimental results for the proposed system. The aim is to realize the hypothesis and verify the performance of the proposed model. The simulation is carried out using PSCAD/EMTDS software. The microgrid system setup considered for both simulation and experimental test is the one illustrated in Figure 1 operating in island mode. Its parameters are listed in Table 1. The same parameters are used for the experimental test setup. The dynamic control performance and system stability for parallel operation of two DERs (namely a supercapacitor and a lead-carbon battery) during power flow changes using the proposed method is demonstrated.

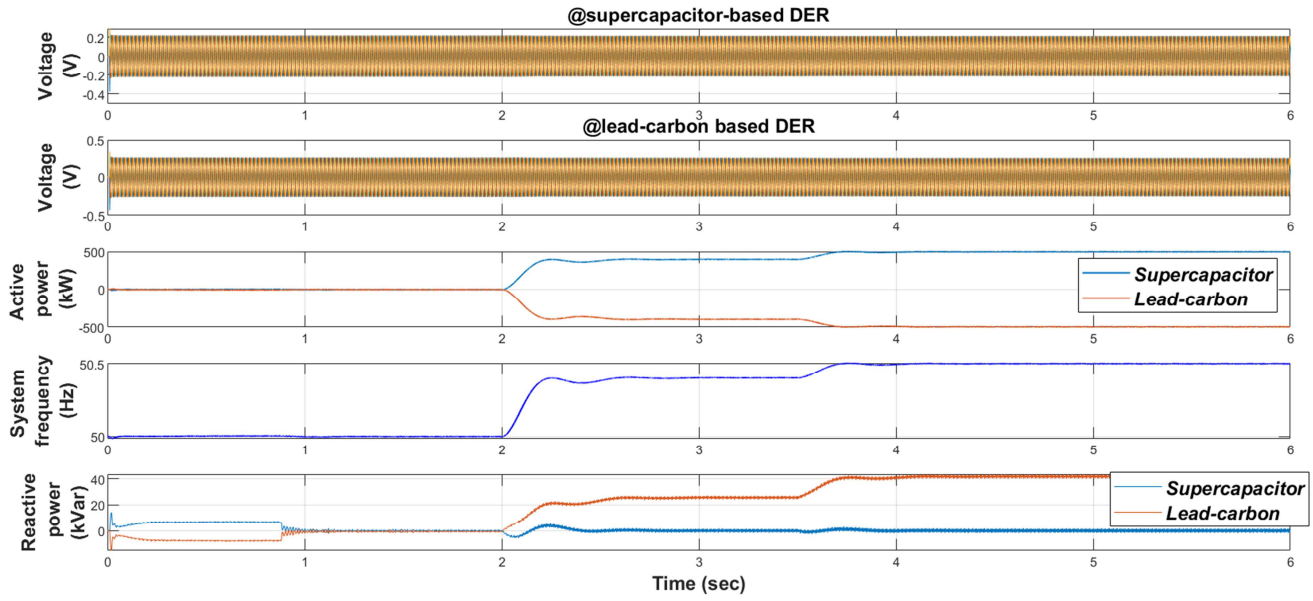

(a)

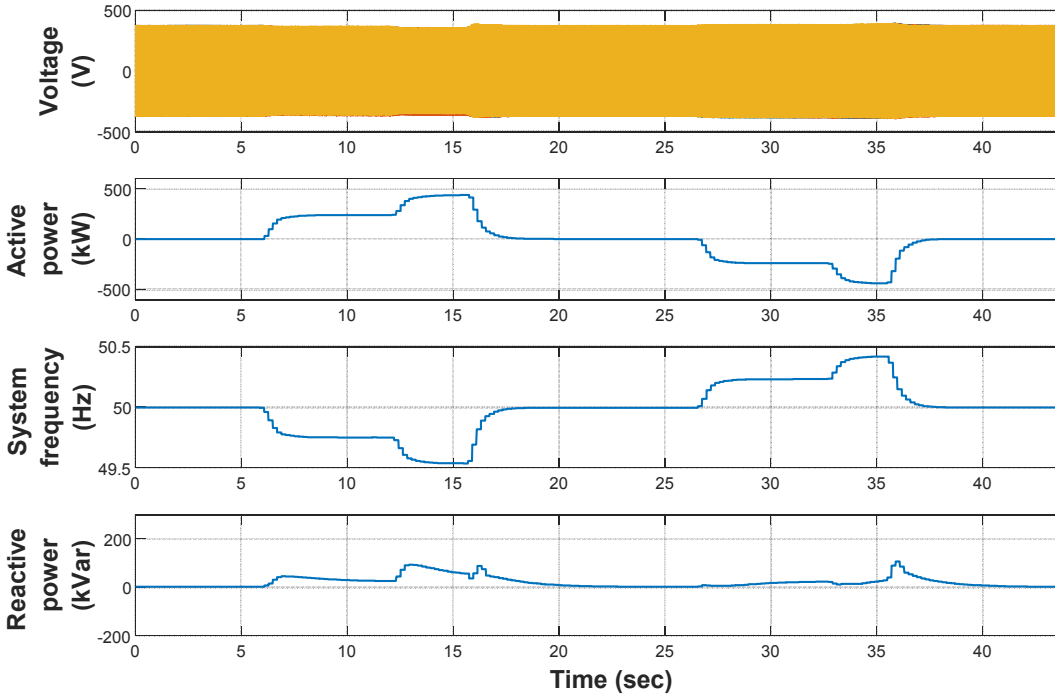

(b)

Figure 24. *Dynamic responses of the system with active damping methods; (a) simulation results, and (b) experimental test results.*

Figures 24(a) and 24(b) respectively show the simulation and experimental test results. The incidence for both the simulation and experimental cases was a change in the amount of power flow. This change was increasing the power from the lead-carbon battery beyond 300kW which is manifested as the boundary of the stable area while the system was operating with only an active damping method1 as shown in Figure 18 and became unstable after that. However, for the realization of the two active methods proposed in this paper, the dynamic stability of frequency and voltage can be guaranteed even when the power flow reaches 500kW.

3.2. Discussion

The results shown in Figure 24 demonstrate that the dynamic responses of voltage, frequency and power flow in both simulation and experimental results are similar. The proposed integrated method has demonstrated superior operational performance and technical advantages compared to conventional methods such as high-order filters [13] and virtual harmonic damper [14]. One of the comparative advantages achieved through the use of the proposed method is the fact that it allows the system to operate in a wide range of frequency spectrum. As presented and analysed in section 2.2, the proposed system can increase the gain and phase margins. The impedance characteristic is also well regulated when the proposed method 1 is incorporated.

The constant function of $G_{ad1}(s)$ is observed to be enough to achieve better impedance characteristics. However, the advantage in improved impedance characteristics, particularly for lower frequencies, comes with an opposite impact on the steady-state stability as the amount of power flow increases further, as verified in the simulation result of Figure 18. Hence, its value should be selected by compromising the impedance characteristics.

In method 2 varying only the value of R_d in $K_{ad2}(s)$ has resulted in a large phase margin due to the high-pass element added to the input of LPF as a filter capacitor voltage-controlled voltage source. However, the method was less beneficial in terms of improvements in impedance characteristics compared with method 1.

The resonance due to LCL type LPF is properly controlled by the proposed methods in this paper. The microgrid can withstand large dynamic disturbances as verified in the simulation and experimental results. The method provides stable operation of the converters under changing equivalent grid impedance values due to changes in operational mode and system arrangement. The method also allows adaptability to the filter parameter alterations.

The current and voltage feedbacks from the output of the LCL filter supplied to the virtual resistance in this active damping method compensates for the voltage deviation due to reactive power differences. It also helps the synchronization between multiple DERs compensating for the possible frequency deviation due to momentary power mismatch when the DERs are being synchronized.

4. Conclusion

This paper presents a novel active damping algorithm for improving the dynamic control of a microgrid composed of converter-based generators. Two active damping methods with

output current feedback and output voltage feedback implemented through damping resistance connected in series and parallel to the LPF capacitance are presented and compared. Constant functional value is chosen and adjusted in the first method just to determine and improve the impedance characteristic of the control-converter-filter system. The mathematical modelling, simulation and experimental verification of the ADA method are provided. When only the first method was implemented, it was observed that the system would become unstable as the amount of power being shared among the DERs increased though there was an improvement in the impedance characteristics. Whereas the ADA method is effective to operate stably with various damping coefficients in a wide range of frequency spectrum. As a result, the resonance is largely damped. To verify the proposed method, the simulation and experimental tests are carried out. The results show that, through the use of the devised ADA method, the voltage and frequency dynamic responses and performance are quite stable and within the acceptable range even with large changes to the power flow in the microgrid.

Acknowledgements

We would like to acknowledge Goldwind Science & Technology Co., Ltd. for supporting this work with funding, materials, and experiments.

References

[1] Benrabah, D. Xu, and Z. Gao, "Active Disturbance Rejection Control of LCL-Filtered Grid-Connected Inverter Using Padé Approximation," *IEEE Trans. Ind. Appl.*, 2018, doi: 10.1109/TIA.2018.2855128.

[2] Wessels, J. Dannehl, and F. W. Fuchs, "Active damping of LCL-filter resonance based on virtual resistor for PWM rectifiers - Stability analysis with different filter parameters," in *PESC Record - IEEE Annual Power Electronics Specialists Conference*, 2008, doi: 10.1109/PESC.2008.4592502.

[3] M. Liserre, F. Blaabjerg, and S. Hansen, "Design and control of an LCL-filter-based three-phase active rectifier," *IEEE Trans. Ind. Appl.*, 2005, doi: 10.1109/TIA.2005.853373.

[4] Y. Guan, Y. Wang, Y. Xie, Y. Liang, A. Lin, and X. Wang, "The Dual-Current Control Strategy of Grid-Connected Inverter with LCL Filter," *IEEE Trans. Power Electron.*, 2019, doi: 10.1109/TPEL.2018.2869625.

[5] J. Dannehl, M. Liserre, and F. W. Fuchs, "Filter-based active damping of voltage source converters with LCL filter," *IEEE Trans. Ind. Electron.*, 2011, doi: 10.1109/TIE.2010.2081952.

[6] W. Wu, Y. Liu, Y. He, H. S. H. Chung, M. Liserre, and F. Blaabjerg, "Damping Methods for Resonances Caused by LCL-Filter-Based Current-Controlled Grid-Tied Power Inverters: An Overview," *IEEE Trans. Ind. Electron.*, 2017, doi: 10.1109/TIE.2017.2714143.

[7] J. Dannehl, F. W. Fuchs, S. Hansen, and P. B. Thøgersen, "Investigation of active damping approaches for PI-based current control of grid-connected pulse width modulation converters with LCL filters," *IEEE Trans. Ind. Appl.*, 2010, doi: 10.1109/TIA.2010.2049974.

[8] W. Ma, Y. Guan, B. Zhang, and L. Wu, "Active Disturbance Rejection Control Based Single Current Feedback Resonance Damping Strategy for LCL-Type Grid-Connected Inverter," *IEEE Trans. Energy Convers.*, 2021, doi: 10.1109/TEC.2020.3006151.

[9] J. Xu, S. Xie, and T. Tang, "Active damping-based control for grid-connected LCL -filtered inverter with injected grid current feedback only," *IEEE Trans. Ind. Electron.*, 2014, doi: 10.1109/TIE.2013.2290771.

[10] X. Wang, F. Blaabjerg, and P. C. Loh, "High-performance feedback-type active damping of LCL-filtered voltage source converters," in *2015 IEEE Energy Conversion Congress and Exposition, ECCE 2015*, 2015, doi: 10.1109/ECCE.2015.7310029.

[11] H. Cha and T. K. Vu, "Comparative analysis of low-pass output filter for single-phase grid-connected photovoltaic inverter," in *Conference Proceedings - IEEE Applied Power Electronics Conference and Exposition - APEC*, 2010, doi: 10.1109/APEC.2010.5433454.

[12] X. Wang, F. Blaabjerg, and P. C. Loh, "Grid-current-feedback active damping for LCL resonance in grid-connected voltage-source converters," *IEEE Trans. Power Electron.*, 2016, doi: 10.1109/TPEL.2015.2411851.

[13] I. Lorzadeh, M. Savaghebi, H. A. Abyaneh, and J. M. Guerrero, "Active damping techniques for LCL-filtered inverters-based microgrids," in *Proceedings - SDEMPED 2015: IEEE 10th International Symposium on Diagnostics for Electrical Machines, Power Electronics and Drives*, 2015, doi: 10.1109/DEMPED.2015.7303722.

[14] Y. W. Li, "Control and resonance damping of voltage-source and current-source converters with LC filters," *IEEE Trans. Ind. Electron.*, 2009, doi: 10.1109/TIE.2008.2009562.